PCCP

Cite this: *Phys. Chem. Chem. Phys.*, 2011, **13**, 4614–4624

www.rsc.org/pccp

**PAPER**

# Dynamics of scattering and dissociative adsorption on a surface alloy: $H_2$/W(100)-$c(2 \times 2)$Cu

**M. N. Batista,[a] H. F. Busnengo[ab] and A. E. Martínez*[ab]**

***Received 15th November 2010, Accepted 4th January 2011***
**DOI: 10.1039/c0cp02542a**

$H_2$ scattering and dissociative adsorption on the W(100)-$c(2 \times 2)$Cu surface alloy is studied based on DFT calculations. A strongly site dependent reactivity is observed in line with results obtained for the density of states projected onto the W and Cu atoms of the topmost layer. $H_2$ dissociation on a defect free terrace of W(100)-$c(2 \times 2)$Cu is found to be a non-activated process like on W(100), despite the reduction of the number of energetically accessible dissociation pathways at low impact energies due to the presence of Cu atoms. A prominence of dynamic trapping and a reduction of the efficacy of trapping to promote dissociation is also verified, leading to a decrease of the initial sticking probability as a function of the molecular impact energy, in qualitative agreement with experimental findings. The heterogeneous reactivity is also evidenced by two different kinds of reflection events at low energies. Its combination gives rise to a broad specular peak superimposed on a cosine-like angular distribution of scattered molecules which is in good agreement with available experimental data.



## I. Introduction

Surface alloys have attracted a great interest during the last years due to their applications in surface chemistry and in the developement of new materials (see ref. 1 and references therein). In view of applications in heterogeneous catalysis, the combination of atoms with different electronic structures might be used to favor the production of a particular reaction product (*i.e.* to increase surface selectivity) or to enhance a global reaction rate, for instance, by stabilizing an active intermediate state (*i.e.* to increase the catalyst efficiency).

The dynamics and kinetics of adsorption/desorption of $H_2$ on/from metal surfaces have been traditionally used as a workhorse to understand some of the elementary steps in heterogeneous catalysis. Thus, many experimental and theoretical studies of $H_2$ interacting with metal surfaces have been carried out during the last years.[2,3] However, the case of $H_2$ interacting with surface alloys has received much less attention specially from the theoretical side. One of the first studies reporting adsorption and scattering probabilities of $H_2$ on a bimetallic surface has dealt with NiAl(110), *i.e.* a surface of an alloy bulk material.[4,5] More recently, new dynamical studies were focussed on the reactivity of complete pseudomorphic monolayers of Cu and Pd deposited on a Ru(0001) substrate and the analysis of the relative role played by strain and ligand effects.[6,7] To our knowledge, there are no reported dynamical studies dealing with stable substitutional surface alloys composed of metals that do not form alloys in bulk. In particular, if the combined metal atoms have very different electronic properties and reactivities, the resulting surface alloy might give rise to properties not easily found in the kind of bimetallic surfaces mentioned above. In view of this, W–Cu appears as an ideal benchmark system for a theoretical investigation. On the one hand, pure W and Cu surfaces have very different reactivities at least as far as the dissociative adsorption probability of $H_2$ is concerned: *e.g.* $H_2$ dissociation is, respectively, non-activated and highly activated ($E_b \approx 0.5$ eV) on all the low Miller index surfaces of W and Cu. On the other hand, W and Cu do not form a bulk alloy but it has been experimentally found that they form a stable substitutional 2D surface alloy when Cu atoms are evaporated on W(100): *e.g.* W(100)-$c(2 \times 2)$Cu.[8] Moreover, the latter surface alloy has been employed in molecular beam experiments in which the $H_2$ sticking probability was determined as a function of H coverage as well as its surface temperature dependence and the angular distribution of the unreactive scattered molecules.[9,10] The main signature of the adsorption dynamics put in evidence by the latter experiments was the prominent role of a dynamic precursor dissociation mechanism (*i.e.* dynamic trapping) which might be responsible for the large dissociative adsorption probability, $P_{diss}$, observed in spite of the apparent absence of direct dissociation at very low impact energies. Still, it was not possible to elucidate, for instance, if for such low impact energies (below $E_i \approx 0.15$ eV) dissociation takes place on terraces or if surface defects (*e.g.* steps) are required.[9,10]

[a] *Instituto de Física Rosario (CONICET-UNR), Av. Pellegrini 250, 2000 Rosario, Argentina*
[b] *Laboratario de Colisiones Atómicas, Facultad de Ciencias Exactas, Ingeniería y Agrimensura, Universidad Nacional de Rosario, Av. Pellegrini 250, 2000 Rosario, Argentina*

 

From the theoretical side, electronic structure calculations of the W(100)-$c(2 \times 2)$Cu surface pointed to a weak bonding between the Cu and W atoms whereas the stability of W(100)-$c(2 \times 2)$Cu was ascribed to a near instability of W(100) under vacancy creation.[11] In a more recent short communication dealing with H and $H_2$ interacting with W(100)-$c(2 \times 2)$Cu, some of us have shown that: (i) the H adsorption energies on top-W and top-Cu sites of W(100)-$c(2 \times 2)$Cu are similar to those obtained on top sites of pure W and Cu surfaces, respectively, and (ii) though the presence of Cu atoms in W(100)-$c(2 \times 2)$Cu reduces significantly the H adsorption energy on the most stable site on W(100) (*i.e.* bridge), there exist non-activated $H_2$ dissociation pathways for molecular configurations (defined by the molecular orientation and the surface site on which the molecular center is placed) that allow the two H atoms of the molecule to separate from each other going simultaneously to favorable adsorption geometries on the surface: *i.e.* on top-W and on hollow sites.[12]

Although these aspects of the H and $H_2$/W(100)-$c(2 \times 2)$Cu PES provide useful information on the reactivity of the W(100)-$c(2 \times 2)$Cu surface for $H_2$ dissociation, dynamics calculations are required to explain the origin of the main signatures of the available experimental data obtained in molecular beam experiments. The objective of this work is to go beyond the restricted static analysis presented in ref. 12, by using classical trajectory calculations based on a continuous representation of the six-dimensional (6D) potential energy surface (PES) obtained by interpolation of the Density Functional Theory (DFT) results. The plan of this paper is the following. In Section II we briefly describe the geometric and electronic properties of the clean W(100)-$c(2 \times 2)$Cu surface as well as the main static signatures of its interaction with atomic and molecular hydrogen. Then, in Section III we present an analysis of the classical trajectory results for the dissociative adsorption probability of $H_2$ (as a function of the impact energy under normal incidence) as well as the angular distribution of unreactive $H_2$ molecules scattered back to vacuum. Finally, in Section IV we summarize the main conclusions of our study.

## II. System characterization

Experimentally, the W(100)-$c(2 \times 2)$Cu surface is prepared by evaporating Cu atoms (*e.g.* at 300 K) onto a W(100) surface followed by annealing to 900 K.[9] This procedure gives rise to a stable two dimensional Cu–W alloy in which every other surface W atom in the topmost layer of W(100) is replaced by a Cu atom.[8,13] Auger electron spectroscopy (AES) measurements have shown that the latter procedure does not give rise to significant bulk alloying[8] whereas Temperature Programed Desorption (TPD), Low Energy Electron Diffraction (LEED) and nitrogen uptake measurements[8,14] showed that the W(100)-$c(2 \times 2)$Cu structure is stable in a relatively large range of Cu coverage around $\Theta_{Cu} = 0.5$.

In order to investigate the interaction of atomic and molecular hydrogen with W(100)-$c(2 \times 2)$Cu we have carried out DFT calculations within the Generalized Gradient Approximation (GGA). We have used the Vienna Ab initio Simulation Package (VASP)[15–19] that employs a plane wave basis set to represent electronic wavefunctions. The electron–ion interaction was described using ultrasoft pseudopotentials[20] and the energy cutoff was set to 230 eV. An electron smearing of $\sigma = 0.4$ eV was introduced within the Methfessel and Paxton approach[21] and the resulting energies were extrapolated for $\sigma \to 0$.

The choice of the exchange and correlation (XC) energy functional to describe the dynamics of molecules interacting with metal surfaces is an important issue. The most widely used XC functionals for such purposes so far have been those proposed by Perdew and Wang (PW91)[22,23] and Hammer *et al.*[24] (RPBE). Whereas PW91 predicts that dissociation of $H_2$ on W(100) is a non-activated process, in line with molecular beam experiments, RPBE calculations give rise to (small) spurious early activation energy barriers.[25] Still, for other molecule/metal systems, both PW91 and RPBE XC functionals seem to be reasonable choices. Moreover, it has been recently shown that an intermediate XC functional expressed as a linear combination of PW91 and RPBE allows us to obtain the best agreement with a large number of experimental data for $H_2$/Cu(111).[26] Therefore, for $H_2$/W(100)-$c(2 \times 2)$Cu we have carried out calculations using both, PW91 and RPBE. However, for brevity we will only show a comparison of the results obtained with both XC functionals when significant differences between them exist.

The DFT-PW91 lattice constant we have obtained for bulk W is $a = 3.17$ Å, in good agreement with the experimental value.[27] The W(100)-$c(2 \times 2)$Cu surface has been represented by a five-layer slab in which the four bottom layers correspond to pure W(100) whereas in the topmost layer, alternate W atoms are replaced by Cu atoms. Thus, the surface alloy's topmost layer has 50–50% of W and Cu atoms and its periodicity is characterized by a $c(2 \times 2)$ unit cell, $a$ being the nearest neighbor distance between topmost layer W and Cu atoms (see Fig. 1).[8,13] Starting from a configuration with all the atoms located at the positions of the W atoms in the ideal unreconstructed W(100) surface, we have carried out a full geometry optimization of the slab. The resulting average height of the topmost layer W (Cu) atoms with respect to the second surface layer, $\Delta_{12}^{W}$ ($\Delta_{12}^{Cu}$), is 1.37 Å (1.46 Å), *i.e.* 13.8% (7.66%) smaller than the ideal bulk W(100) interlayer distance, $a/2$. Thus, the W(100)-$c(2 \times 2)$Cu slab is characterized by a

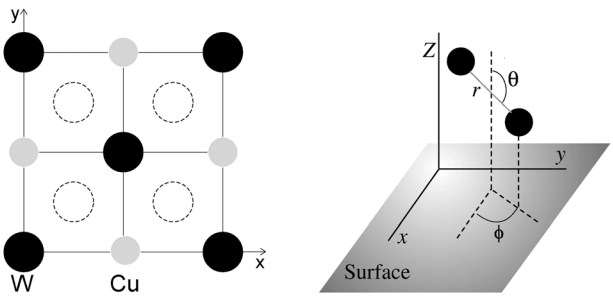


**Fig. 1** Left panel: schematic picture of the surface W(100)-$c(2 \times 2)$Cu cell used in the calculations for the bcc(100) surface. Black (W) and grey (Cu) circles correspond to the atoms in the topmost layer while white circles represent W atoms in the second layer. Right panel: coordinates definition for $H_2$ molecules near the surface.

rumpling of only $\sim$0.1 Å of its topmost layer. The rumpling of lower layers is even smaller ($\leq$0.06 Å) and the corresponding interlayer distances differ from the ideal bulk W(100) value by less than 2%.

### A Electronic structure of W(100)-$c(2 \times 2)$Cu

In order to understand the origin of the most significant features of the $H_2$/W(100)-$c(2 \times 2)$Cu interaction, it is useful to investigate first the electronic structure of the clean surface alloy. Though this has been already done by other authors in the past,[11] according to our purposes, it is convenient to do it using the same level of theory as employed to describe the $H_2$–surface interaction, *i.e.* DFT-GGA. To inspect the Cu–W bonding in W(100)-$c(2 \times 2)$Cu we have computed the local density of states projected onto the topmost layer W (W-PDOS) and Cu (Cu-PDOS) atoms. In order to illustrate how electronic states centered on Cu and W atoms are modified due to the formation of the Cu–W bonds, we have carried out PDOS calculations for several heights of the Cu *layer* above its equilibrium position in the surface alloy (between $Z_{Cu} = 0$ and $Z_{Cu} = 4$ Å). The results for $Z_{Cu} = 4$ Å, 1 Å and 0 [*i.e.* for the equilibrium geometry of W(100)-$c(2 \times 2)$Cu] are, respectively, shown in the panels a, b, and c of Fig. 2. For $Z_{Cu} = 4$ Å (Fig. 2a), the shortest Cu–Cu and Cu–W distances are large (*i.e.* 6.34 Å and 5.18 Å respectively). Thus, the open Cu overlayer barely interacts with the underlying W(100) substrate that presents a $c(2 \times 2)$ periodic arrangement of vacancies, W(100)-$c(2 \times 2)_v$. As a consequence, the Cu-centered electronic states preserve their atomic character as shown by the sharp peak of Cu-PDOS at $E_F - 1$ eV, $E_F$ being the Fermi energy. The W-PDOS is broad and extends from $\sim E_F - 3.3$ eV to $E_F + 1.5$ eV, as for the case of W(100) (not shown).

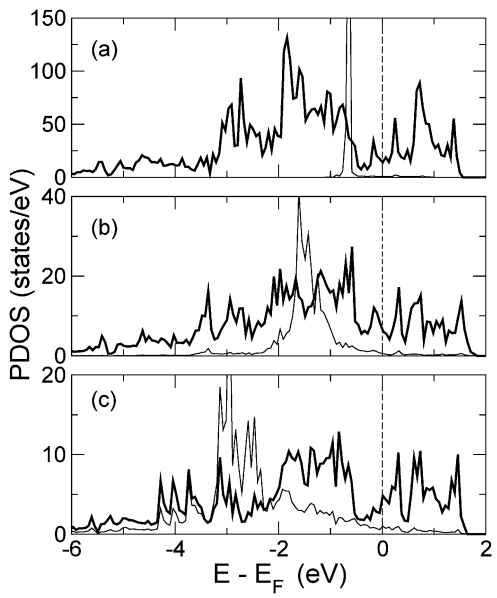


**Fig. 2** PDOS for W atoms (thick line) in the topmost layer of the surface alloy and Cu atoms (thin line) with (a) $Z_{Cu} = 4$ Å, (b) $Z_{Cu} = 1$ Å, (c) $Z_{Cu} = 0$. (equilibrium geometry). The Fermi energy is indicated by the vertical dashed line. W-PDOS are multiplied by appropriate constants in order to be displayed together with Cu-PDOS but comparable between them.

When $Z_{Cu}$ decreases (see *e.g.* Fig. 2b, *i.e.* $Z_{Cu} = 1$ Å) the Cu-PDOS peak shifts down and broadens as expected due to the interaction of the Cu atomic states with the broad band of the W(100)-$c(2 \times 2)_v$ *substrate*. This also entails some changes of the W-PDOS, in particular the loss of states around $E_F - 1.9$ eV and the appearance of new features at the bottom of the W-projected band at $\sim E_F - 3.4$ eV.

When the Cu atoms are in their equilibrium position for W(100)-$c(2 \times 2)$Cu, *i.e.* $Z_{Cu} = 0$ (Fig. 2c), the shift down of the Cu-PDOS curve is more pronounced. Other significant changes with respect to the case of $Z_{Cu} = 1$ Å are the broadening of the main Cu-PDOS peak that now extends from $\sim E_F - 3.2$ eV to $E_F - 2.1$ eV, the appearance of three peaks at $\sim E_F - 4.3$ eV, $\sim E_F - 4.0$ eV and $\sim E_F - 3.7$ eV and a broad shoulder above $E_F - 2.$ eV (decreasing with increasing energy).

The main Cu-PDOS peak between $\sim E_F - 3.2$ eV and $E_F - 2.1$ eV is less broadened than the d band of pure Cu surfaces [*e.g.* Cu(100)[6]]. This indicates that the Cu d states in the surface alloy are more strongly localized than in pure Cu surfaces which indicates a relatively weak W–Cu bond consistent with the fact that W and Cu do not form stable bulk alloys.

The fact that the three peaks at $\sim E_F - 4.3$ eV, $\sim E_F - 4.$ eV and $\sim E_F - 3.7$ eV appear in both Cu-PDOS and W-PDOS (Fig. 2c) indicates that they correspond (at least partially) to electrons shared by Cu and top-most layer W atoms. The analysis of the *lm*- and *l*-selective PDOS presented in Fig. 3 shows that the latter peaks are, in fact, associated with the bond between: (i) Cu $d_{x2}$ orbitals with topmost layer W s orbitals and second layer W d orbitals (at $E_F - 3.7$ eV), (ii) Cu s orbitals with topmost layer W $d_{x2}$ orbitals and second layer W d orbitals (at $E_F - 4.3$ eV), and (iii) Cu $d_{x2}$ orbitals with topmost layer W $d_{x2}$ orbitals and second layer W d orbitals (at $E_F - 4.0$ eV).

Finally, the Cu-LDOS shoulder above $E_F - 2.0$ eV receives contributions from the bonding between Cu d states and various W d states but a clear *lm*-selective identification is

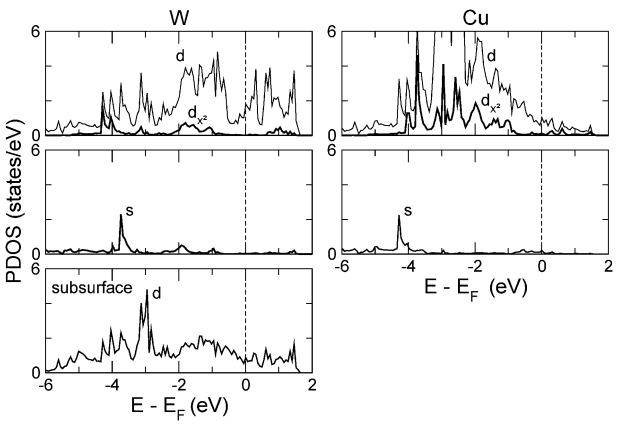


**Fig. 3** First and second rows: thick lines, PDOS for projection onto $d_x^2$ and s orbitals; thin lines, PDOS for projection onto d states, for W (left) and Cu (right) atoms on the W(100)-$c(2 \times 2)$Cu topmost layer. Third row: PDOS for projection onto d states, for W atoms in the subsurface layer of W(100)-$c(2 \times 2)$Cu. The Fermi energy is indicated by the vertical dashed line.

 

more difficult because in that energy region there is contribution from all the W d states in the W(100)-$c(2 \times 2)_v$ surface.

The very different shapes of the W-PDOS and Cu-PDOS suggest a strongly site dependent reactivity of the surface alloy, at least as far as regions around top-W and top-Cu sites are concerned. On the one hand, the center of the Cu-PDOS well below the Fermi level and the small density of states at the Fermi level point to a low reactivity of the surface alloy around top-Cu sites. On the other hand, the fact that in W(100)-$c(2 \times 2)$Cu (Fig. 2c) the W-PDOS is broad and extends from well below the Fermi level up to $\sim E_F + 1.5$ eV, as in the case of both W(100)-$c(2 \times 2)_v$ (Fig. 2a) and W(100) (not shown), suggests that the high reactivity for H and $H_2$ adsorption (at least around top-W sites) of the pure W surfaces should barely change due to the presence of Cu atoms in the surface alloy. In fact, the W–Cu bond weaker than the W–W bonds in W(100) might entail an even higher reactivity in the case of the surface alloy.

### B H/surface and $H_2$/surface interactions

All the calculations for H and $H_2$ interacting with W(100)-$c(2 \times 2)$Cu were carried out for a $2 \times 2$ (6.34 Å $\times$ 6.34 Å) square unit cell (Fig. 1) and with a vacuum space between consecutive slabs of $\sim$15 Å. A $5 \times 5 \times 1$ mesh of $k$-points was chosen according to the Monkhorst and Pack method[28] to sample the Brillouin zone.

In a previous short communication some of us have already reported site dependent DFT-PW91 H adsorption energies and some $H_2$ dissociation pathways on W(100)-$c(2 \times 2)$Cu.[12] Thus, here we will only briefly summarize the main results of ref. 12 to focus mainly on the description of the dynamics.

We define the atomic hydrogen adsorption energy on a site X, as follows

$$E_{ads}^{X} = -[E^{X}(\text{H/surface}) - E(\text{H}) - E(\text{surface})] \qquad (1)$$

where $E$(H) and $E$(surface) are the total energies of H in vacuum (spin unrestricted calculation) and of the clean surface, respectively, and $E^X$(H/surface) is the total energy of the H/surface system for H in its equilibrium height above the surface on site X. In contrast with H/W(100) for which bridge is the most favorable adsorption site ($E_{ads}^{bridge} = 3.1$ eV), for H/W(100)-$c(2 \times 2)$Cu the most stable sites are top-W and hollow, with almost the same adsorption energy $E_{ads}^{hollow} \approx E_{ads}^{top\text{-}W} = 2.7$ eV, the optimum H heights above the surface on top-W and hollow being 1.75 Å and 0.5 Å respectively.[12] On top-Cu, we have obtained $E_{ads}^{top\text{-}Cu} = 2.0$ eV, for the H atom located 1.62 Å above the Cu layer. Both the adsorption energy and geometry are very similar to the DFT results found for H adsorbed on top-Cu sites on a pure Cu low Miller index surface.[29–32]

To summarize, the replacement of 50% of W atoms by Cu atoms entails a change of the most stable adsorption geometry and a reduction of the adsorption energy by $\sim$0.4 eV, but still, dissociative adsorption remains an exothermic process after Cu deposition on W(100).

Fig. 4 shows three 2D($Z$,$r$) cuts of the $H_2$/W(100)-$c(2 \times 2)$Cu 6D-PES for the molecule approaching flat on the surface on top-Cu (a) and top-W (b) sites as well as for a tilted

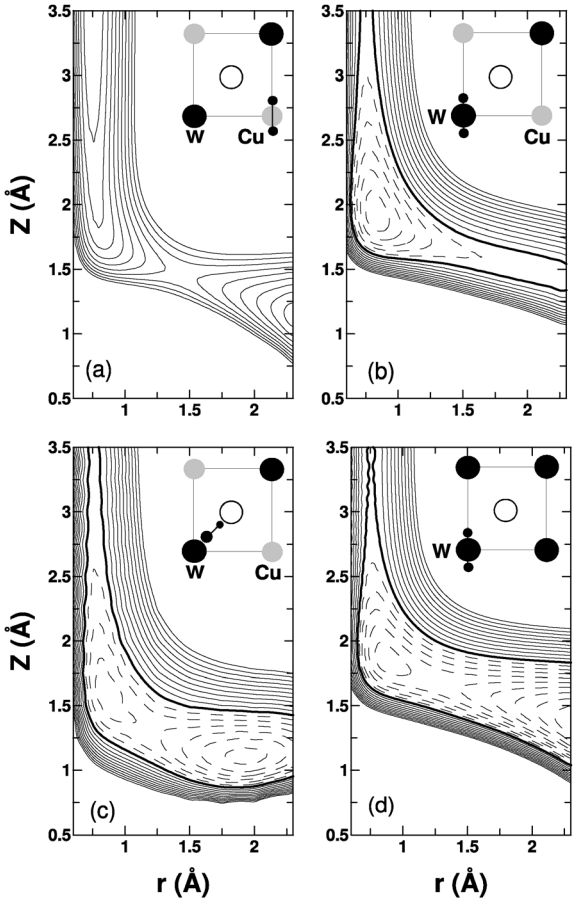


**Fig. 4** DFT results for 2D($Z$,$r$) cuts of the PES corresponding to an $H_2$ molecule for different sites and molecular orientations (a) top-Cu, $\theta = 90°$, $\phi = 90°$; (b) top-W, $\theta = 90°$, $\phi = 90°$; (c) mid-point between top-W and hollow, $\theta = 45°$, $\phi = 135°$ all on W(100)-$c(2 \times 2)$Cu; (d) top-W, $\theta = 90°$, $\phi = 90°$ on W(100). Distance between equipotential lines is $\Delta E = 0.1$ eV. The reference energy level $E = 0$ is indicated with a thick line and those for which $E < 0$ by dashed lines.

configuration allowing the molecule to dissociate, with both H atoms going towards the optimum adsorption geometries on top-W and hollow sites (c). In Fig. 4d we have also included a 2D($Z$,$r$) cut of the $H_2$/W(100) PES on top-W in order to further illustrate the effect of alloying W(100) with half monolayer of Cu atoms.

On top-W the attractive character of the PES that characterizes the $H_2$ interaction with W(100) in the entrance channel is barely changed by the presence of Cu atoms in W(100)-$c(2 \times 2)$Cu (see Fig. 4b and d). However, Cu atoms introduce some *repulsion* around them that gives rise to a significant increase of the potential energy in the exit channel on top-W [not observed for $H_2$/W(100)] due to the smaller $E_{ads}^{bridge}$ value in the alloy. It is expected that this feature of the PES will be very efficient promoting dynamic trapping for low energy impinging molecules initially attracted toward top-W sites. The 2D($Z$,$r$) cuts of the PES for $H_2$ on top-Cu sites (see *e.g.* Fig. 4a) present a large late activation barrier of $\sim$0.7 meV, very similar to the one found in the case of pure Cu surfaces (see *e.g.* ref. 31). The very strongly site dependent reactivity of W(100)-$c(2 \times 2)$Cu for $H_2$ dissociation, as well as

the small changes in the atomic adsorption energies and the $H_2$/surface interaction in the entrance channel on top-W and top-Cu sites with respect to W(100) and pure Cu surfaces are fully consistent with the main signatures of the PDOS of the clean surface alloy discussed above.

In spite of the overall reduction of reactivity provoked by the presence of Cu atoms, $H_2$ dissociative adsorption on W(100)-$c(2 \times 2)$Cu is still a non-activated process like on pure W(100). This is clearly illustrated by Fig. 4c in which we show the 2D($Z$,$r$) cut of the PES for $X = \frac{a}{4}$, $Y = \frac{a}{4}$ (the mid-point between top-W and hollow) and $\theta = 135°$, $\phi = 45°$. This geometry is particularly convenient for dissociation on the surface alloy because it allows the H atoms to separate from each other going towards the optimum atomic adsorption geometries on top-W ($Z \approx 1.75$ Å) and hollow ($Z \approx 0.5$ Å) sites.

The DFT-RPBE calculations predict a smaller reactivity of the W(100)-$c(2 \times 2)$Cu surface with respect to PW91: *e.g.* smaller H adsorption energies and higher $H_2$ activation energy barriers for dissociation (see below). However, the $H_2$/W(100)-$c(2 \times 2)$Cu PES still presents non-activated dissociation pathways, for instance, for the molecular configuration considered in Fig. 4c. Thus our DFT results unambiguously show that the replacement of half of topmost layer W atoms by Cu is not enough to completely turn *unreactive* the W(100) surface since W(100)-$c(2 \times 2)$Cu still presents non-activated pathways for $H_2$ dissociation.

Though the latter information is relevant for qualitatively characterizing the W(100)-$c(2 \times 2)$Cu surface reactivity for $H_2$ dissociative adsorption, a quantitative evaluation requires dynamic calculations for which the knowledge of the full 6D PES is needed. In the following section we briefly describe the interpolation procedure we have employed to obtain such a continuous representation of the PES using the corrugation reducing procedure (CRP).[33]

**1 PES interpolation.** The present implementation of the CRP is very similar to the one applied previously for a surface offering 50–50% of different metal atoms in its outermost layer, *i.e.* $H_2$/NiAl(110).[34] The 6D interpolation function, $\mathscr{I}^{6D}$ is defined as:

$$\mathscr{I}^{6D}(X,Y,Z,r,\theta,\phi) = V_{6D}(X,Y,Z,r,\theta,\phi) - [V_{3D}(X_1,Y_1,Z_1) + V_{3D}(X_2,Y_2,Z_2)]$$

where $X,Y,Z$ ($X_i,Y_i,Z_i$) defines the position of the molecular center of mass (of the $i$th H atom), $r$ is the H–H distance and $\theta,\phi$ determines the molecular orientation (Fig. 1). The H/surface potential, $V_{3D}$, is written as follows

$$V_{3D}(X,Y,Z) = \mathscr{I}^{3D}(X,Y,Z) + \sum_{i=1}^{N_W} V_{1D}^{W}(|R-R_i|) + \sum_{i=1}^{N_{Cu}} V_{1D}^{Cu}(|R-R_i|)$$

where the $V_{1D}^{W}$ and $V_{1D}^{Cu}$ pairwise potentials have been taken from the $Z$-dependent H/surface potential on top-W and top-Cu sites respectively.[33,34] $\mathscr{I}^{3D}(X,Y,Z)$ was interpolated using 3D cubic splines. For $\mathscr{I}^{6D}(X,Y,Z,r,\theta,\phi)$ we have first used 2D-cubic splines to interpolate over $Z$ and $r$ for each molecular configuration, then, symmetry adapted expansions of trigonometric functions were employed for the interpolation over $\theta$ and $\phi$ on each surface site and finally, 2D-periodic cubic spline was used to interpolate over $X$ and $Y$.

Input H/surface DFT-PW91 interaction energies were computed on the nine surface sites: $\{(X = i\frac{a}{4}, Y = 0), i = 0,1,2,3,4\}$, $\{(X = i\frac{a}{4}, Y = \frac{a}{4}), i = 1,2,3\}$ and $(X = \frac{a}{2}, Y = \frac{a}{2})$, from $Z = -1.25$ Å to $Z = 5.25$ Å (step equal to 0.25 Å). To interpolate $\mathscr{I}^{6D}$, we have carried out DFT-PW91 calculations for 49 2D($Z$,$r$) cuts of the PES with the molecular center of mass on the latter nine surface sites: 9 vertical configurations ($\theta = 0$), 19 horizontal configurations ($\theta = \pi/2$), and 21 tilted configurations ($\theta = \pi/4$). For each 2D ($Z$,$r$) cut we have employed a $15 \times 13 = 195$ point grid for 0.5 Å $\leq Z \leq$ 4.0 Å and 0.4 Å $\leq r \leq$ 2.3 Å. As usual, we have defined the zero value of the $H_2$/surface interaction energy for the molecule far from the surface (in the middle of the vacuum space) and for the H–H equilibrium distance in vaccuum (*i.e.* $r = 0.75$ Å).

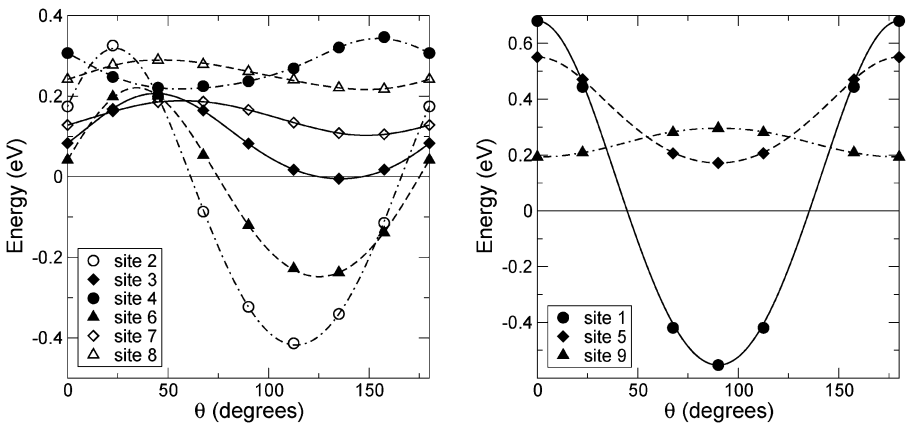


**Fig. 5** $H_2$/surface interaction for a given set ($X,Y,Z,r,\theta,\phi$), as a function of $\theta$. For sites 1 (top-W), 3 (bridge), 5 (top-Cu), 7 (mid-point between bridge and hollow) and 9 (hollow): $\phi = 0°$. For site 2 (mid-point between top-W and bridge) and 4 (mid-point between top-Cu and bridge): $\phi = 90°$. For site 6 (mid-point between top-W and hollow): $\phi = 135°$ and for site 8 (mid-point between top-Cu and hollow): $\phi = 45°$. Z = 2 Å, $r = 0.8$ Å for all the cases. Lines correspond to results obtained by interpolation of the 6D-PES while symbols are *ab initio* calculations.

 

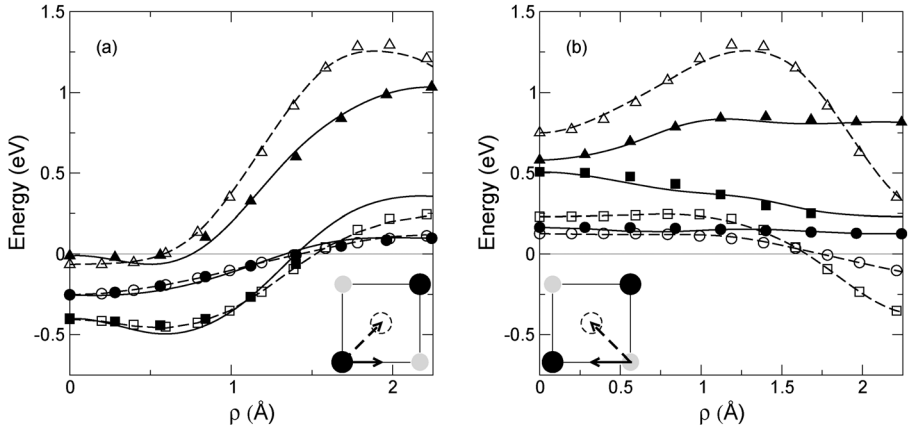


**Fig. 6** $H_2$/surface interaction for a given set $(X,Y,Z,r,\theta,\phi)$, displayed as a function of $\rho = \sqrt{X^2 + Y^2}$. Circles: $Z$ = 2.5 Å, $r$ = 0.8 Å; squares: $Z$ = 1.75 Å, $r$ = 0.8 Å; triangles: $Z$ = 1.5 Å, $r$ = 1.75 Å. Lines correspond to interpolation results and symbols to *ab initio* calculations. (a) Straight lines and full symbols: top W → bridge for $\theta = \phi = 90°$; dashed lines and empty symbols: top W → hollow for $\theta = 90°$ and $\phi = 135°$. (b) Straight lines and full symbols: top Cu → bridge for $\theta = \phi = 90°$; dashed lines and empty symbols: top Cu → hollow for $\theta = 90°$ and $\phi = 45°$. The dashed and straight lines in the diagrams below illustrate the different pathways.

Extra DFT-PW91 calculations were carried out for configurations not included in the input data set in order to assess the accuracy of the interpolated PES (see Fig. 5 and 6). Concerning the $\theta$-dependence of the PES on surface sites for which there are DFT-PW91 data in the input data set (Fig. 5) the deviations are always lower than 20 meV. The largest errors in the $X,Y$-dependence (Fig. 6) in the low energy region of interest for the dynamics are slightly larger (*i.e.* ~45 meV). In addition, it is important to note that all the trends of the DFT-PW91 data are perfectly reproduced by the interpolated PES. Thus, the errors of the interpolated DFT-PW91 6D PES are perfectly acceptable for our purposes.

**2 Influence of the XC functional: PW91 and RPBE choices.** To quantify to what extent the main characteristics of the DFT-PW91 6D PES described in the previous subsection change if the RPBE XC functional is employed instead of PW91, we have also carried out DFT-RPBE calculations for $H_2$/W(100)-$c(2 \times 2)$Cu. In agreement with previous similar comparisons for other $H_2$/metal-surface systems,[26,35,36] the RPBE PES is slightly less reactive than the PW91 one. We have found that for $H_2$/W(100)-$c(2 \times 2)$Cu, a good approximation of the DFT-RPBE PES (througout the low energy region of the configuration space visited by low impact energy molecules) can be obtained from the PW91 PES by simply adding a repulsive term that depends only on the molecule/surface distance $Z$:

$$V^{\mathrm{RPBE}} = \begin{cases} V^{\mathrm{PW91}}, & \text{if } Z \geq Z_2 \\ V^{\mathrm{PW91}} + \Delta V^{\mathrm{RPBE}} \left[\frac{1}{2} + \frac{1}{2}\cos\left(\pi \frac{(Z - Z_1)}{(Z_2 - Z_1)}\right)\right] & \text{if } Z_1 < Z < Z_2 \\ V^{\mathrm{PW91}} + \Delta V^{\mathrm{RPBE}} & \text{if } Z \leq Z_1 \end{cases} \quad (2)$$

with $\Delta V^{\mathrm{RPBE}}$ = 0.3 eV, $Z_1$ = 0.5 Å, $Z_2$ = 3 Å.

Fig. 7 clearly shows that the RPBE PES obtained in this way provides a very good representation of the DFT-RPBE data for molecular configurations on four different surface sites. Even more important is the fact that in spite of the lower overall reactivity of the RPBE PES, the main signatures of the PW91 PES [*e.g.* the heterogeneous reactivity on top-W and top-Cu sites and the existence of non-activated pathways for the dissociation of $H_2$ on W(100)-$c(2 \times 2)$Cu] remain unchanged.

## III. Dynamical study

### A Dissociative adsorption

We have employed both the PW91 and the RPBE PES for classical trajectory calculations for initially non-rotating $H_2$ molecules impinging on W(100)-$c(2 \times 2)$Cu at normal incidence for initial translational kinetic energies $0 \leq E_i \leq 0.5$ eV. For such relatively low initial energies, the only open scattering channels are dissociative adsorption and elastic or rotationally inelastic scattering. Dissociation was considered to take place whenever the internuclear distance reached the value $r_{\mathrm{diss}}$ = 2.3 Å with $\mathrm{d}r/\mathrm{d}t > 0$ and trajectories were considered as reflected when they reached the initial height above the surface (*i.e.* $Z$ = 5 Å) with a velocity of the center of mass pointing to the vacuum. Thus, dissociative adsorption (reflection) probabilities were simply computed as the ratio of the number of trajectories leading to dissociation (reflection) and the total number of computed trajectories (typically ~5000).

Our objective is to investigate dissociative adsorption and unreactive scattering of $H_2$ initially in its vibrational ground state. It is well known that using classical trajectory calculations, some attention must be payed to the initial vibrational zero point energy (ZPE) of $H_2$, in particular, in order to evaluate $H_2$ adsorption probabilities.[37] On one hand, if the initial vibrational ZPE is not taken into account as in the so-called classical (C) calculations, the contribution of the direct dissociation channel is underestimated because the effect of vibrational softening cannot be accounted for. On the other hand, for non-activated dissociation, calculations taking into account the initial vibrational ZPE of $H_2$ (*i.e.* usually referred to as quasi-classical, QC) quench indirect dynamic trapping-mediated dissociation because of some energy transfer from vibrational motion to translational degrees of freedom not

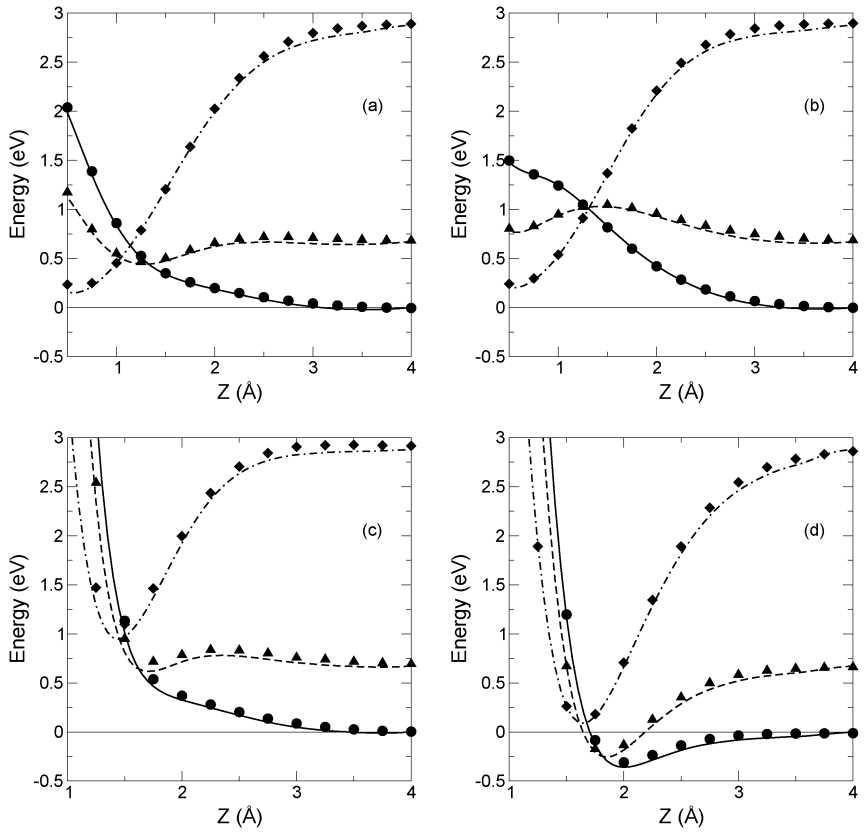


**Fig. 7** Comparison of PW91-PES and RPBE-PES results for the $H_2$/surface interaction displayed as a function of Z for: (a) bridge, $\theta = 90°$, $\phi = 90°$, (b) hollow, $\theta = 90°$, $\phi = 0°$; (c) top-Cu, $\theta = 90°$, $\phi = 0°$ and (d) top-W, $\theta = 90°$, $\phi = 0°$. circles and straight lines: $r = 0.75$ Å; triangles and dashed lines: $r = 1$ Å; diamonds and dot-dashed lines: r = 1.5 Å. Symbols correspond to RPBE-DFT calculations and lines display the results for the RPBE-PES obtained by adding a repulsive term to the PW91-PES, as stated in eqn (2).

allowed in quantum calculations. A method, usually referred to as CZPE, that has allowed us to obtain dissociation probabilities in good agreement with quantum calculations for $H_2$/Pd(111) consists in running C calculations (*i.e.* without vibrational ZPE) but adding to the PES a negative (attractive) term $\Delta ZPE(Z)$, to account for vibrational softening effects that translate into additional acceleration of the impinging molecules in the entrance channel.[37] In the present CZPE calculations, we have used:

$$\Delta ZPE(Z) = \begin{cases} 0 & \text{if } Z \geq Z_{max} \\ -0.140\,\text{eV}\left[\frac{1}{2}+\frac{1}{2}\cos\left(\pi\frac{(Z-Z_{min})}{(Z_{max}-Z_{min})}\right)\right] & \text{if } Z_{min} < Z < Z_{max} \\ -0.140\,\text{eV} & \text{if } Z \leq Z_{min} \end{cases} \quad (3)$$

with $Z_{min} = 1.5$ Å and $Z_{max} = 3.0$ Å.

In Fig. 8 we show the dissociative adsorption probability, $P_{diss}$, of $H_2$ on W(100)-$c(2 \times 2)$Cu as a function of the initial impact energy, $E_i$, obtained in C and CZPE calculations using both the PW91-PES (Fig. 8a and b) and the RPBE-PES (Fig. 8c and d). In what follows, we will denote with $P^{T}_{diss,XC}$ the dissociative adsorption probability obtained in T = C,CZPE calculations using the XC = PW91,RPBE PES.

Irrespective of the XC-PES employed, both $P^{C}_{diss,XC}$ and $P^{CZPE}_{diss,XC}$ present a pronounced non-monotonic $E_i$-dependence in agreement with the experimental results represented by solid circles.[10] Such a behavior in the theoretical results arises from the combination of two dissociation mechanisms: direct and dynamic trapping. Here, we have associated dissociation events with each mechanism, depending on the number of rebounds, $n_{reb}$, undergone by each trajectory before dissociation.[37] Direct dissociation was associated with reactive trajectories after $n_{reb} < 5$ and dynamic trapping mediated dissociation was considered to take place when $n_{reb} \geq 5$. The panels of Fig. 8 also show the contribution to $P^{T}_{diss,XC}$ coming from the direct and dynamic trapping mediated dissociation mechanisms. The direct dissociation probability increases when $E_i$ increases and the converse is obtained for the dissociation after dynamic trapping.

As expected from eqn (3), the less attractive character of the RPBE PES translates into lower values of $P_{diss}$ than for PW91 PES for both C and CZPE calculations. Theoretical adsorption probabilities tend to overestimate the experimental data, the results obtained with the RPBE PES being the closest to the experiments. In addition, the $E_i$ values for which the minima of the $P_{diss}$ curves are obtained for the RPBE PES are closer to the experimental one ($\sim$0.15 eV) than in the case of the PW91 PES. Interestingly, the $P^{C}_{diss,RPBE}(E_i)$ curve is in almost perfect agreement with experiments. However, such a

 

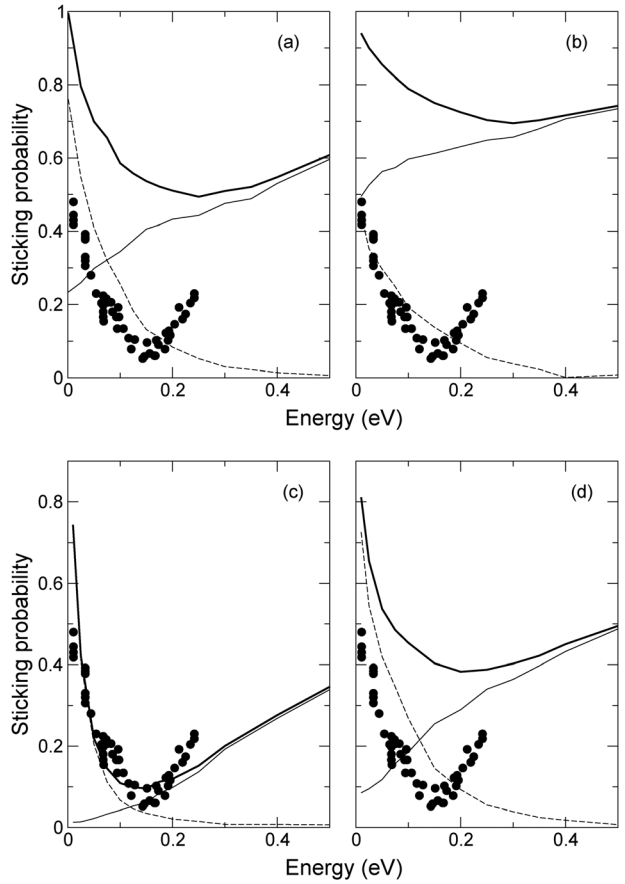


**Fig. 8** Sticking probability for $H_2$ molecules on W(100)$c(2 \times 2)$Cu, as a function of the impact energy. Theoretical results correspond to (a) PW91-C; (b) PW91-CZPE; (c) RPBE-C and (d) RPBE-CZPE calculations. Thick full line: total dissociative adsorption probability; thin full line: direct contribution; dashed line: indirect contribution. Full circles: experimental results.[10]

quantitative agreement might be simply fortuitous because for this system that presents a strong attraction in the entrance channel on top-W sites followed by late activation energy barriers, vibrational softening (not accounted for by C calculations) is expected to play an important role.

Regardless of the XC PES employed to describe the $H_2$/W(100)-$c(2 \times 2)$Cu interaction, at low energies we have obtained a very important role of dynamic trapping as a promotor of dissociative adsorption. This is fully consistent with the interpretation of the dissociation dynamics at low energies proposed by Butler and Hayden.[9] The knowledge of the full six-dimensional PESs and the analysis of the classical trajectory calculations also allow us to identify the origin of such behavior. The presence of Cu atoms in the alloy not only introduces surface regions where dissociation is largely activated (around top-Cu and hollow sites[12]) but also creates moderate late barriers for dissociation for molecular configurations with the molecular center of mass on top-W sites. Therefore, a large fraction of low energy impinging $H_2$ molecules are initially efficiently attracted towards top-W sites (as in the case of $H_2$/W(100), see Fig. 4d) but the late activation barriers introduced by the presence of Cu atoms tend to hinder dissociation. Thus, although direct dissociation events do exist at low energies (even for the less reactive RPBE PES), for instance, for molecules aproaching the surface around the mid-point between top-W and hollow sites (see Fig. 4c), a large fraction of trajectories remain dynamically trapped for a while before reaching an energetically available pathway toward dissociation.

Based on an estimated onset of direct dissociation at 0.15 eV, Butler and Hayden proposed that $H_2$ dissociation on a perfect (defect-free) terrace of W(100)-$c(2 \times 2)$Cu surface might be an activated process, and that low energy dissociation events would only take place at surface defects.[10] Though some enhancement of dissociative adsorption due to the presence of steps cannot be ruled out, our results clearly show that dissociative adsorption at low impact energies can take place also on the large terraces of the alloy surface. Thus, according to the present results, the apparent onset of direct dissociation observed experimentally at $E_i \approx 0.15$ eV seems to be simply a dynamical effect associated with a small probability of finding the few existing non-activated dissociation pathways at low energies.

Before concluding this section, it is important to mention that the values of $P_{diss}$ obtained in QC results (not shown) are, respectively, higher and lower than those obtained in C and CZPE calculations above $E_i \approx 0.1$ eV (for which direct dissociation prevails), and present an almost monotonic $E_i$-dependence (because of the quenching of dynamic trapping) at lower impact energies. To elucidate what is the most convenient way to carry out classical trajectory calculations (*i.e.* C, CZPE or QC) in order to compare with the experimental sticking probabilities, 6D quantum (Q) dynamical calculations (using the same PESs) are desirable. Such Q calculations are already in progress and will be presented elsewhere. Still, the role played by both dynamic trapping and also the direct dissociation mechanisms, as put in evidence by the previous analysis, will be hardly modified by Q effects. Moreover, the inclusion or not in the classical trajectory calculations of the vibrational ZPE, in general, does not affect the angular distribution of scattered molecules[38] that will be considered in what follows.

### B Non-reactive scattering

For $H_2$ with its center of mass near top-W sites, the strong attraction in the entrance channel followed by late activation energy barriers for dissociation provokes dynamic trapping whose efficiency to promote dissociation of low energy molecules is high but still far from 100%. Therefore, a large fraction of initially trapped molecules come back to vacuum instead of finding an energetically accessible dissociation pathway. This certainly affects the angular distribution of molecules scattered back to vacuum.[39,40] Therefore, in this section we analyse the angular distribution of $H_2$ scattered back to vacuum from W(100)-$c(2 \times 2)$Cu and we compare our results with the experiments of ref. 9.

All the theoretical results reported below have been obtained in C calculations and using the RPBE PES but it is important to mention that very similar results are also found in CZPE and QC calculations (and also using the PW91 PES). Then, the choice of C calculations and the RPBE PES is simply

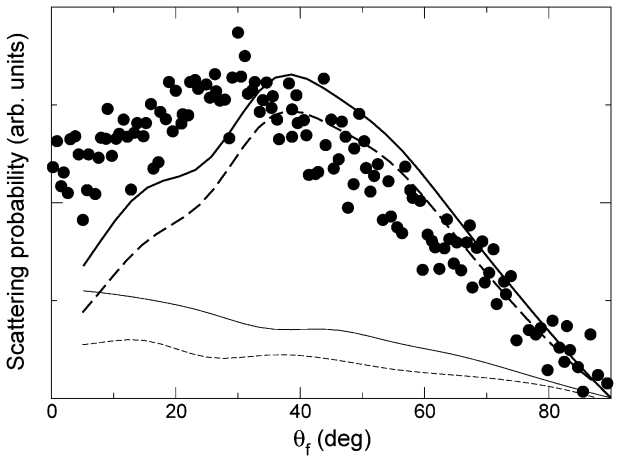


**Fig. 9** Scattering probabilities as a function of the scattering angle $\theta_f$ for $H_2$ molecules impinging on a W(100)$c(2 \times 2)$Cu surface along the [100] direction, for an incident angle $\theta_i = 48^\circ$ and an energy of 68 meV. Filled circles: measured scattering distribution.[10] Thick full line: theoretical results; thick dashed line: theoretical results for molecules reflected after less than 5 rebounds (direct contribution); thin dashed line: theoretical results for molecules reflected after 5 rebounds (indirect contribution); thin full line: theoretical results for molecules reflected with outgoing trajectory in the perpendicular [110] plane.

because the larger reflectivity obtained in such calculations allows us to obtain acceptable statistical errors with a smaller number of trajectories. In order to compute the angular distribution of scattered molecules in-plane we have integrated $10^5$ trajectories for each particular incidence condition considered.

In Fig. 9 we show the angular distribution of $H_2$ molecules scattered in-plane from W(100)-$c(2 \times 2)$Cu for $E_i = 68$ meV, angle of incidence with respect to the surface normal, $\theta_i = 48^\circ$, and incidence direction [100] (see Fig. 1). The thick full line corresponds to the total distribution of scattered molecules and the dashed thick and thin lines correspond to the fraction of reflected trajectories with $n_{reb} < 5$ (associated with direct scattering) and $n_{reb} \geq 5$ (associated with a dynamic trapping–desorption mechanism) respectively. It is important to mention that 84% of the trajectories associated with direct scattering are reflected after only a single rebound and the average number of rebounds for reflected trajectories temporarily trapped is 26. Whereas direct scattering gives rise to a broad sub-specular peak at $\theta_f = 40^\circ$, indirect scattering is characterized by a cosine distribution. The latter in-plane angular distribution is very similar to the total angular distribution of trajectories scattered back to vacuum perpendicular to the scattering plane defined by the incidence direction and the surface normal (thin full line in Fig. 9). This is a consequence of a complete memory loss of scattered trajectories after more than 5 rebounds near the surface which entails a random angular distribution of reflected trajectories. We also emphasize that similar signatures of the angular distributions of scattered molecules have been also obtained for other set of (low) initial impact energies and incidence angles.

Interestingly, the theoretical angular distribution of in-plane scattered molecules is in good agreement with experiments.[10] Still, the cosine component in the experimental distribution is slightly larger than the theoretical one which might be due to some contribution in experiments, from molecules desorbing recombinatively after dissociation.[10]

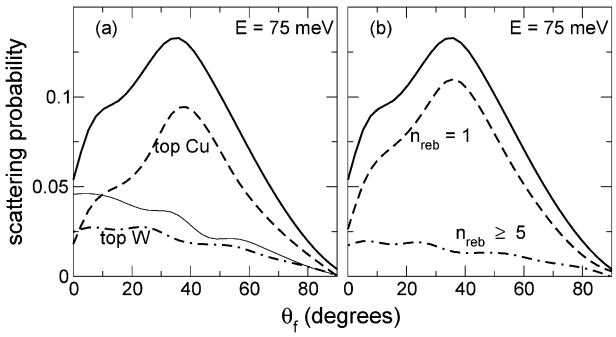


**Fig. 10** Scattering probabilities as a function of the scattering angle $\theta_f$ for $H_2$ molecules on a W(100)$c(2 \times 2)$Cu surface along the [100] direction, for an incident angle $\theta_i = 40^\circ$. (a) Full line: total in-plane scattering probability; dashed line: scattering probabilities corresponding to the top Cu region; dash and dot line: scattering probabilities corresponding to the top W region; thin full line: total scattering probability for trajectories outcoming in the [110] direction. (b) Full line: total in-plane scattering probability; dashed line: scattering probabilities corresponding to molecules reflected after one rebound; dash and dot line: scattering probabilities corresponding to molecules reflected after 5 rebounds.

For a further characterization of trajectories contributing to the two scattering mechanisms mentioned above, we have also recorded the coordinates of the molecular center of mass for the configuration closest to the surface along each unreactive (scattered) trajectory $(X_{ref}, Y_{ref}, Z_{ref})$. This allowed us to separate, for instance, trajectories being scattered back to vacuum near top-W and top-Cu sites. The analysis of the latter results shows that there is not only a strong correlation between the angular distribution of scattered molecules with the number of rebounds but also with the region of the surface where unreactive trajectories are scattered back to vacuum. This is illustrated in Fig. 10, where we show (for $E_i = 0.075$ eV, $\theta_i = 40^\circ$) the total angular distribution of in-plane scattered molecules as well as the partial angular distributions for trajectories scattered back to vacuum near top-Cu and top-W atoms (panel a) and with $n_{reb} = 1$ and $n_{reb} \geq 5$ (panel b). These results clearly show that at low energies, molecules scattered back to vacuum from W(100)-$c(2 \times 2)$Cu with a cosine-like distribution have been temporarily trapped near top-W sites whereas molecules preferentially scattered in a broad angular region around the specular peak have undergone a single collision with the surface around top-Cu sites. Still, it is important to emphasize that the presence of Cu atoms on the surface alloy is mainly responsible for the cosine distribution associated with reflection near top-W sites because of the appearance of late barriers that prevent dissociation of low energy molecules approaching the surface near top-W sites. For higher $E_i$ values, the fraction of reflected trajectories temporarily trapped decreases because dynamic trapping does and accordingly, the cosine and specular components of the angular distribution of scattered molecules in-plane decrease and increase respectively.

Further evidence of a clear spatial separation of scattering mechanisms on the W–Cu surface alloy at low energies is

 

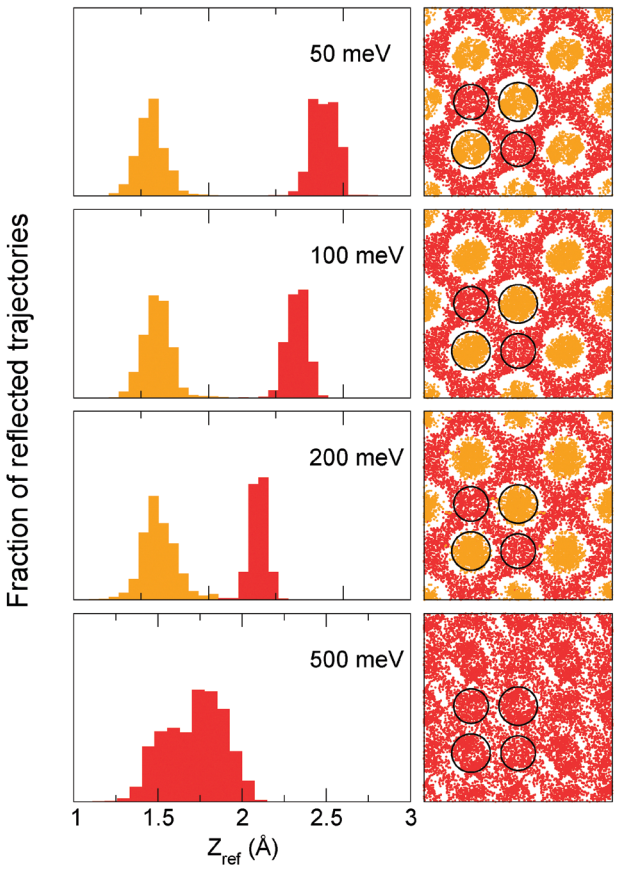


**Fig. 11** Distribution of the distance of closest approach for molecules scattered at normal incidence, for different energies. The right panel corresponds to the position where reflection takes place over the surface, dark circles: molecules being reflected far from the surface, light circles: molecules reflected close to the surface. Open circles indicate the W atoms and Cu atoms.

provided by Fig. 11 which shows the distribution of $Z_{ref}$ for various values of $E_i$ for normal incidence ($\theta_i = 0$). For $E_i = 50$ meV we obtained a bimodal distribution of $Z_{ref}$ with one of the peaks centered around 2.75 Å [dark peak] and the other around 1.6 Å [light peak]. This bimodal shape of the $Z_{ref}$-distribution is also obtained for higher impact energies but when $E_i$ increases, the peak located at larger $Z_{ref}$ values goes down. Thus, for $E_i = 500$ meV the total distribution transforms into a single broader peak centered at $Z_{ref} = 1.75$ Å. It is important to emphasize that such a bimodal $Z_{ref}$-distribution is unusual because it differs from the one obtained for many other surfaces including NiAl(110) (*i.e.* another example of a surface combining 50–50% of reactive and unreactive species).[41]

In the right panels of Fig. 11, we also show the $X_{ref} - Y_{ref}$ distributions and we have used light and dark circles to distinguish the trajectories contributing to each peak of the bimodal distribution (the position of the topmost layer W and Cu surface atoms is represented by circles centered on the top-W and top-Cu sites respectively). It is clear that the bimodal distribution obtained for $E_i$ values lower than ~300 meV is a direct consequence of trajectories being reflected at two different regions of the alloy surface. The peak at large $Z_{ref}$ values corresponds to reflection (after a single rebound) on top-Cu and hollow sites, around which the $H_2$/W(100)-$c(2 \times 2)$Cu PES is repulsive early in the entrance channel.[12] When $E_i$ increases, $H_2$ molecules can approach closer to the surface even on these less reactive surface sites, as a consequence the peak centered at larger values of $Z_{ref}$ approaches the surface and the bimodal character of the distribution disappears. In contrast, the peak of the $Z_{ref}$-distribution centered at 1.6 Å is related to reflection (after a large number of rebounds) around top-W sites due to an initial attraction towards the surface and the existence of late barriers due to the presence of the less reactive Cu atoms. For instance, for impact energies of 50, 100 and 200 meV $\langle n_{reb} \rangle \simeq$ 38, 11.5 and 4.5, respectively. For $E_i = 0.5$ eV, $\langle n_{reb} \rangle$ is only slightly greater than 1 irrespective of surface area where reflections have taken place because dynamic trapping becomes negligible.

## IV. Conclusions

We have presented a theoretical study of the dynamics of $H_2$ scattering and dissociative adsorption on the W(100)-$c(2 \times 2)$Cu surface alloy based on Density Functional Theory (DFT) calculations. In line with the results of the density of states projected (PDOS) onto the topmost layer W and Cu atoms, we have found a strongly site dependent reactivity of the surface for $H_2$ dissociative adsorption. On top-Cu sites dissociation is highly activated, as on pure Cu surfaces, whereas on top-W the initial attraction towards the surface [characteristic of pure W surfaces like W(100)] is preserved but the presence of Cu atoms entails (small) late activation energy barriers. Though the fraction of non-activated pathways is strongly reduced due to the presence of Cu atoms, $H_2$ dissociation on a defect free terrace of W(100)$c(2 \times 2)$Cu is a non-activated process like on W(100). The reduction of the number of energetically accessible dissociation pathways at low impact energies provokes a prominence of dynamic trapping and a reduction of the efficacy of trapping to promote dissociation. These two main features of the $H_2$/W(100)$c(2 \times 2)$Cu PES are, respectively, responsible for (i) a prominent initial decrease of the initial sticking probability as a function of the molecular impact energy, $E_i$, and (ii) an important cosine-like component in the angular distribution of scattered low energy $H_2$ molecules.

A highly heterogeneous *reactivity* of this surface alloy, predicted by the analysis of the PDOS calculations, is put in evidence by two different kinds of reflection events that are identified at low energies: (a) direct reflection that takes place far from the surface around top-Cu sites, and (b) reflection through a trapping–desorption mechanism that takes place near top-W sites and entails a much closer approach of the impinging molecules to the surface. The combination of these two reflection mechanisms gives rise to a broad specular peak superimposed on a cosine-like angular distribution of scattered molecules which is in good agreement with available experimental data.

Concerning the behavior of the initial sticking probability, the values of the probabilities appear sensitive to: (i) the choice of the exchange–correlation (XC) used in the DFT calculations, and (ii) the way the initial vibrational energy of the molecules

is taken into account in classical trajectory calculations. However, in our description its non-monotonic $E_i$ dependence is also in good agreement with experiments. Whereas the XC improvement requires further progress and/or developments of new XC functionals, the second issue points to a need of quantum dynamical calculations which are now in progress and will be presented elsewhere.

## Acknowledgements

This work has been supported by ANPCyT-Argentina (Project No. PICT 33595).

## References


1 B. E. Hayden and A. Hodgson, *J. Phys.: Condens. Matter*, 1999, **11**, 8397.
2 G. J. Kroes, *Science*, 2008, **321**, 794.
3 C. Luntz, *Chemical Bonding at Surfaces and Interfaces*, Elsevier, Amsterdam, 2008.
4 P. Rivière, H. F. Busnengo and F. Martín, *J. Chem. Phys.*, 2005, **123**, 74705.
5 D. Farías, R. Miranda and K. H. Rieder, *J. Chem. Phys.*, 2002, **117**, 2255.
6 G. Laurent, H. F. Busnengo, P. Rivière and F. Martín, *Phys. Rev. B: Condens. Matter*, 2008, **77**, 193408.
7 G. Laurent, C. Díaz, H. Busnengo and F. Martín, *Phys. Rev. B: Condens. Matter*, 2010, **81**, 161404.
8 G. Attard and D. King, *Surf. Sci.*, 1987, **188**, 589.
9 D. A. Butler and B. E. Hayden, *Chem. Phys. Lett.*, 1995, **232**, 542.
10 D. Butler and B. E. Hayden, *Surf. Sci.*, 1995, **337**, 67.
11 D. A. Singh and H. Krakauer, *Surf. Sci.*, 1989, **216**, 303.
12 A. E. Martínez, W. Dong and H. F. Busnengo, *Appl. Surf. Sci.*, 2007, **254**, 82.
13 E. Bauer, H. Poppa, G. Todd and F. Bonczek, *J. Appl. Phys.*, 1974, **45**, 5164.
14 G. A. Attard and D. A. King, *J. Chem. Soc., Faraday Trans.*, 1990, **86**, 2735.
15 G. Kresse and J. Hafner, *Phys. Rev. B: Condens. Matter*, 1993, **47**, 558.
16 G. Kresse and J. Hafner, *Phys. Rev. B: Condens. Matter*, 1994, **49**, 14251.
17 G. Kresse and J. Hafner, *J. Phys.: Condens. Matter*, 1994, **6**, 8245.
18 G. Kresse and J. Furthmüller, *Comput. Mater. Sci.*, 1996, **6**, 15.
19 G. Kresse and J. Furthmüller, *Phys. Rev. B: Condens. Matter*, 1996, **54**, 11169.
20 D. Vanderbilt, *Phys. Rev. B: Condens. Matter*, 1990, **41**, 7892.
21 M. Methfessel and A. T. Paxton, *Phys. Rev. B: Condens. Matter*, 1989, **40**, 3616.
22 J. P. Perdew, *Electronic Structure of Solids '91*, ed. P. Ziesche and H. Eschring, Akademie-Verlag, Berlin, 1991.
23 J. P. Perdew and Y. Wang, *Phys. Rev. B: Condens. Matter*, 1992, **45**, 13244.
24 B. Hammer, L. Hansen and J. Nørskov, *Phys. Rev. B: Condens. Matter*, 1999, **59**, 7413.
25 H. F. Busnengo and A. E. Martínez, *J. Phys. Chem. C*, 2008, **112**, 5579.
26 C. Díaz, E. Pijper, R. A. Olsen, H. F. Busnengo, D. Auerbach and G. J. Kroes, *Science*, 2009, **326**, 832.
27 W. P. Davey, *Phys. Rev.*, 1925, **26**, 736.
28 H. Monkhorst and D. Pack, *Phys. Rev. B: Solid State*, 1976, **13**, 5186.
29 K. Strömquist, L. Bengtsson, M. Persson and B. Hammer, *Surf. Sci.*, 1998, **397**, 382.
30 C. Bae, D. Freeman, J. D. Doll, G. Kresse and J. Hafner, *J. Chem. Phys.*, 2000, **113**, 6926.
31 A. Salin, *J. Chem. Phys.*, 2006, **124**, 104704.
32 J. N. H. Xiao and X. Zu, *Chem. Phys.*, 2006, **321**, 48.
33 H. F. Busnengo, A. Salin and W. Dong, *J. Chem. Phys.*, 2000, **112**, 7641.
34 P. Rivière, H. F. Busnengo and F. Martín, *J. Chem. Phys.*, 2004, **121**, 751.
35 M. Luppi, R. A. Olsen and E. J. Baerends, *Phys. Chem. Chem. Phys.*, 2006, **8**, 688.
36 J. K. Vincent, R. A. Olsen, G. J. Kroes, M. Luppi and E. J. Baerends, *J. Chem. Phys.*, 2005, **122**, 044701.
37 H. F. Busnengo, C. Crespos, W. Dong, J. C. Rayez and A. Salin, *J. Chem. Phys.*, 2002, **116**, 9005.
38 C. Díaz, H. F. Busnengo, F. Martín and A. Salin, *J. Chem. Phys.*, 2003, **118**, 2886.
39 M. A. Di Césare, H. F. Busnengo, W. Dong and A. Salin, *J. Chem. Phys.*, 2003, **118**, 11226.
40 D. Barredo, G. Laurent, C. Díaz, P. Nieto, H. F. Busnengo, A. Salin, D. Farías and F. Martín, *J. Phys. Chem. B*, 2006, **125**, 051101.
41 D. Farías, H. F. Busnengo and F. Martín, *J. Phys.: Condens. Matter*, 2007, **19**, 305003.


 